JOURNAL OF GUIDANCE, CONTROL, AND DYNAMICS
Vol. 18, No. 4, July–August 1995

Flutter Margin Augmentation Synthesis Using Normalized Coprime Factors Approach

Dario H. Baldelli* and Hirobumi Ohta†
Nagoya University, Nagoya 464, Japan
and
Hiroshi Matsushita,‡ Masataka Hashidate,§ and Kenichi Saitoh¶
National Aerospace Laboratory, Mitaka, Tokyo 181, Japan

This research is concerned with the design of a flutter margin augmentation system at a supercritical flutter condition subject to control capacity constraints. The control law is synthesized using the H_∞ loop-shaping method at the normalized coprime factors framework, and order reduction processes are applied to both the nominal plant and the synthesized controller. The effects of output weighting on the control capacity and the influence of the controller suboptimality over its reduction process are further investigated. Robust stability analyses dealing with unstructured uncertainties and sensitivity studies by variation of the fundamental flutter parameters are presented. In transonic wind-tunnel tests, the resulting fourth-order digital controller extends the closed-loop flutter dynamic pressure of an aeroservoelastic wing model by 11.4% over its open-loop value, despite discrepancies in the analytically predicted flutter parameters.

Nomenclature

B_1	= process noise distribution matrix
g	= gravity acceleration
$K_\Phi S(s)$	= gain from output disturbance to controller output
$K_\Phi SG(s)$	= gain from input disturbance to controller output
$S(s)$	= gain from output disturbance to plant output
$SG(s)$	= gain from input disturbance to plant output
W	= intensity matrix
η	= zero-mean Gaussian white-noise process

I. Introduction

CURRENT design philosophies in transport wings place emphasis on reducing induced or shock wave drag in order to develop a more fuel-efficient aircraft. Wing span increment and/or uses of supercritical airfoils usually increase loads and decrease the flutter margins.[1] Therefore, if active control principles are incorporated at the beginning of the design process, full advantages from these philosophies would be obtained without the addition of weight for stiffness increase purposes. Hence, an active flutter margin augmentation (FMA) system can be understood as a means to improve the flutter margins when the original flutter speed remains outside the normal operating flight envelope.

From control theory point of view, aeroservoelastic models are governed by modeling uncertainty and loop bandwidth constraints. The latter feature is due to actuator bandwidth limitations and sensor locations (right-half-plane zeros), whereas uncertainties are produced due to inevitable unmodeled high-frequency elastic modes and oscillatory aerodynamic approximation errors in the transonic regime. Accordingly, the essential duty for the control law shall be to stabilize the aeroservoelastic plant as well as maintain the closed-loop stability against unmodeled dynamic and parameter variations while keeping track of the control power capacity. In other words, aeroservoelastic problems ask for controller synthesis procedures in which closed-loop stability is assured and the presence of uncertainties must be taken into account during the controller design stage.

Received March 15, 1994; revision received Sept. 8, 1994; accepted for publication Sept. 12, 1994.

*Graduate Student, Aeronautical Department.
†Associate Professor, Aeronautical Department. Member AIAA.
‡Director for Special Research. Member AIAA.
§Head, Advanced Aircraft Research Group.
¶Researcher, Advanced Aircraft Research Group.

In the past, several methodologies for gust load alleviation and flutter suppression control law synthesis have been employed, and some of them were successfully tested. It is noted, however, that none of them take explicit consideration of uncertainties. Among these, the aerodynamic energy method,[2] the traditional pole/zero loci design,[3] linear quadratic Gaussian (LQG) theory,[4–7] and eigenspace techniques[8] can be mentioned. In addition, NASA recently conducted the active flexible-wing program[9] by using some of these methodologies with favorable results.

In this research we investigate the application of the H_∞ loop-shaping design method at the normalized coprime factors framework[10–12] for the synthesis of a FMA digital control system. In the synthesis process, the uncertain plant model is described in terms of a nominal plant model and a specified uncertainty region, which is represented by stable additive factors to the plant's coprime description. Performance objectives are incorporated with the loop-shaping principle,[13] and a robust stabilization problem is solved for an extended plant at the normalized coprime factors framework.

Since this synthesis methodology leads to high-order dynamic controllers, here the nominal plant and the synthesized controller were subject to order reduction processes in order to facilitate its implementation in an integrated flight control system. The nominal plant order reduction was executed by balanced truncation approximation (BTA) techniques, whereas the controller reduction process was performed by a combined procedure of residualization and the BTA method. In addition, to check the control law robust characteristics, closed-loop parameter sensitivity studies and robust stability analyses by frequency-domain indicators have been performed with the synthesized reduced-order H_∞ controller.

Finally, to validate the designed control laws, this methodology was applied to an aeroservoelastic wind-tunnel model developed at the National Aerospace Laboratory (NAL) and a series of tests have been carried out in the transonic wind tunnel.[14]

This paper is structured as follows. In Sec. II the aeroservoelastic modeling for the wind-tunnel model and its order reduction are described. In Sec. III the controller design methodology is stated and the control law is synthesized. Section IV outlines the controller two-stage order reduction procedure, and Sec. V presents simulation and experimental closed-loop results. A summary is given in Sec. VI.

II. Aeroservoelastic Modeling

The aeroservoelastic wing is a model actively controlled by leading- and trailing-edge control surfaces. The wing model has seven points for strain gauge allocations at which the bending and

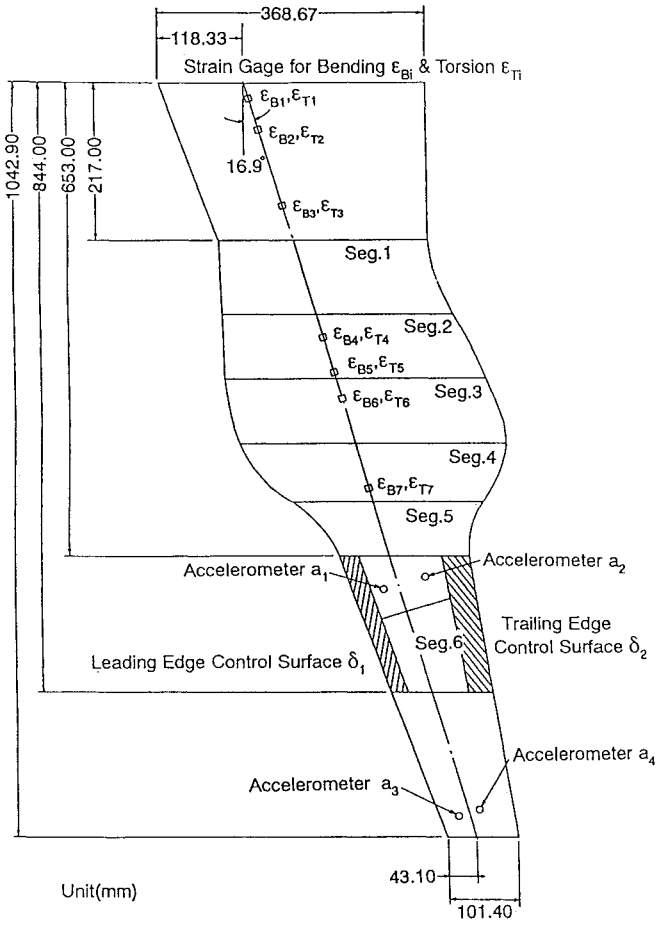

Fig. 1 Aeroservoelastic wing model.

torsional strains can be simultaneously measured. Also, four accelerometers were fixed, one near each surface hinge line and the others near the wing-model tip, as shown in Fig. 1. The transonic wing model can be considered as a scaled, high-aspect-ratio supercritical wing to be used for high-efficiency commercial aircraft. High-performance alternating-current (AC) servomotors are accommodated inside the wing planform, which results in an inflated central section configuration. The trailing-edge control surface and its near accelerometer sensor were selected in this study, resulting in a single-input, single-output (SISO) plant.

To formulate the aeroelastic equations of motion, the flexible mode shapes, natural frequencies, and damping coefficients derived from a finite element modal analysis were corrected using ground vibration test data. Given that the transonic flutter is a highly nonlinear phenomenon, which is difficult to be characterized in a simple formulation, this study computed the unsteady aerodynamic forces as a function of the Mach number and the reduced frequencies using the subsonic lifting surface method of double t point.[15] These generalized forces are described in the frequency domain,[16] where a single lag factor term was used to idealize the time delay inherent in unsteady aerodynamic loading. Clearly, this approach introduces aerodynamic model uncertainties with which the controller synthesis methodology must deal.

The actuator unit dynamics description was derived from frequency response test data and modeled over a wide frequency range as a second-order system with a bandwidth of 40 Hz. As will be stated below, its response lag characteristics dictated restrictions on the rms control surface deflections and its rate of change, respectively.

The overall open-loop aeroservoelastic system at a prescribed dynamic pressure can be written in state-space form as

$$\dot{x} = Ax + B\delta_c + B_1\eta$$
$$x = [\xi^T \quad \delta^T \quad \dot{\xi}^T \quad \dot{\delta}^T \quad \pi^T]^T, \qquad E[\eta\eta^T] = W\delta(t-\tau) \tag{1}$$

The process noise based on previous wind-tunnel tests is used to evaluate the control surface activity, taking into account the influence of the transonic wind-tunnel turbulence over the wing model. The state vector consists of N structural elastic modes ξ, one actuator state δ, their respective rates of change ($\dot{\xi}$ and $\dot{\delta}$), and the N augmented aerodynamic states π. The total number of states becomes $n = 3N + 2$. In addition, the gravity contribution to the vertically fastened wing model is considered in the output equation[5]

$$a_2 = \sum_{i=1}^{N} \phi_i(x_2, y_2)\ddot{\xi}(t) - g\sum_{i=1}^{N} \frac{\partial}{\partial y}\phi_i(x_2, y_2)\xi(t) \tag{2}$$

where $\phi_i(x_2, y_2)$ depends on the mode shapes at the accelerometer location. The observable output used for feedback purposes can be expressed by the states and control variable as

$$y = Cx + D\delta_c \tag{3}$$

The frequencies of the first four elastic modes ($N = 4$), which play an essential role in the flutter phenomenon, are located at 13.62, 36.00, 41.88, and 84.62 Hz, respectively. The mathematical model predicts that the wing model becomes unstable at the dynamic pressure qf_{ol} of 23.89 kPa with a flutter frequency at 24.3 Hz. The elastic modes and actuator unit roots are displayed in Fig. 2 as a function of velocity, which ranges from 10 to 360 m/s with intervals of 10 m/s. As can be observed, the flutter modes are characterized by merging frequencies of the first elastic (bending) and second elastic (coupled bending and torsional) modes, which are changed to mode shapes composed of important contributions of both of them.

Since the phase lag generated by one step time delay (sampling frequency of 500 Hz) achieves 20 deg at the flutter frequency, it seems unrealistic to neglect the influence of this effect. Therefore, the inclusion of an antialiasing filter at 75 Hz and a first-order Padé filter were considered in order to assure equivalent performances between continuous and digital controllers. Consequently, the final aeroservoelastic model results in a 16th-order plant, e.g., $n = 16$.

Design Objectives and Specifications

The primary design objective is to extend the open-loop flutter dynamic pressure boundary at Mach 0.8 by 20% (supercritical flutter condition) within allowable control surface activity. The rms control surface deflection is prescribed to be lower than 1 deg and its rate less than 90 deg/s when evaluated with the wind-tunnel disturbance model at the supercritical flutter condition.

Aeroservoelastic-Model Reduction

Applying the BTA method[17] on the normalized left coprime factors of the model, an order reduction was performed on the model. The BTA realizations were obtained by using Schur decomposition of the controllability and observability Gramians of the model. Succinctly, when the states are converted into internally balanced ones, they have controllability and observability Gramians that are equal and diagonal. The diagonal elements are the Hankel singular values and form a set of closed-loop input-output invariants.[18] After discarding those states of negligible value, the final set of equations maintains the most important input-output characteristics of the system. The order reduction method has an easily computed error bound in terms of the truncated Hankel singular values.[19] That is, if the reduced-order model $G_r(s)$ is obtained by the BTA method, then

$$\|G(s) - G_r(s)\|_\infty \le 2\sum_{i=k+1}^{n} \sigma_i \tag{4}$$

where $\sigma_1 \ge \sigma_2 \ge \cdots \ge \sigma_k \ge \sigma_{k+1}$ are the associated Hankel singular values of $G(s)$.

Consequently, five states were removed, which can be associated with the four unsteady aerodynamic approximation states and the 75-Hz antialiasing filter state. Figure 3 shows that a scarcely visible difference exists at the low-frequency region in gain and phase plots, but it fits very well at frequencies where the flutter phenomenon is characterized. It is worth mentioning that the reduced plant of 11th

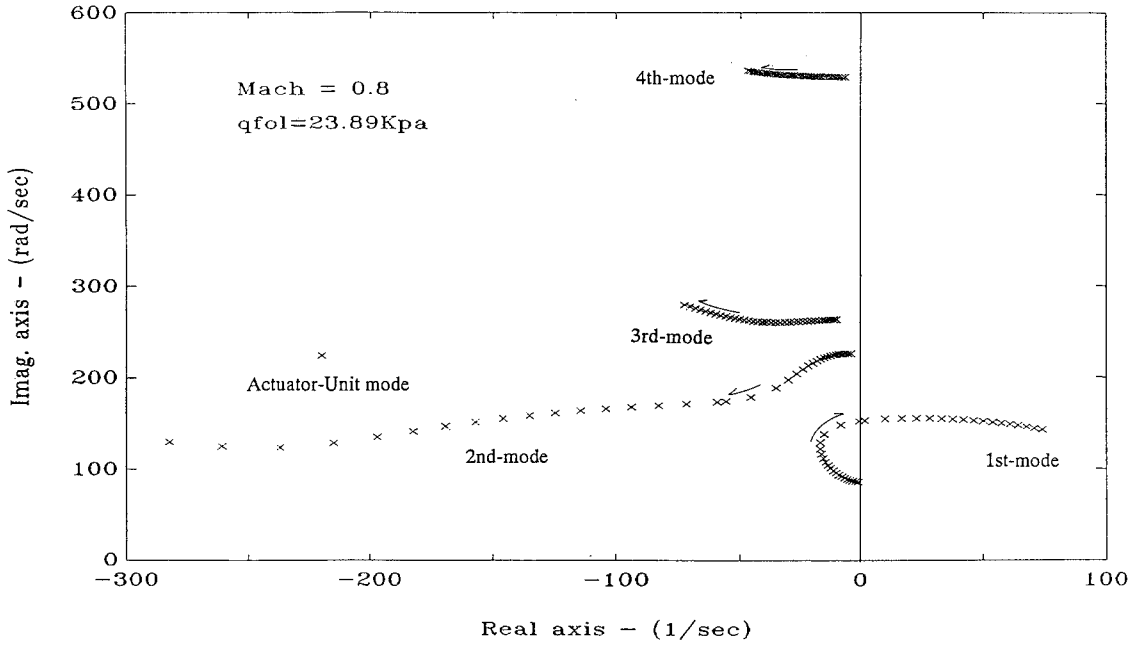

Fig. 2 Open-loop aeroservoelastic root locus (10 m/s velocity intervals).

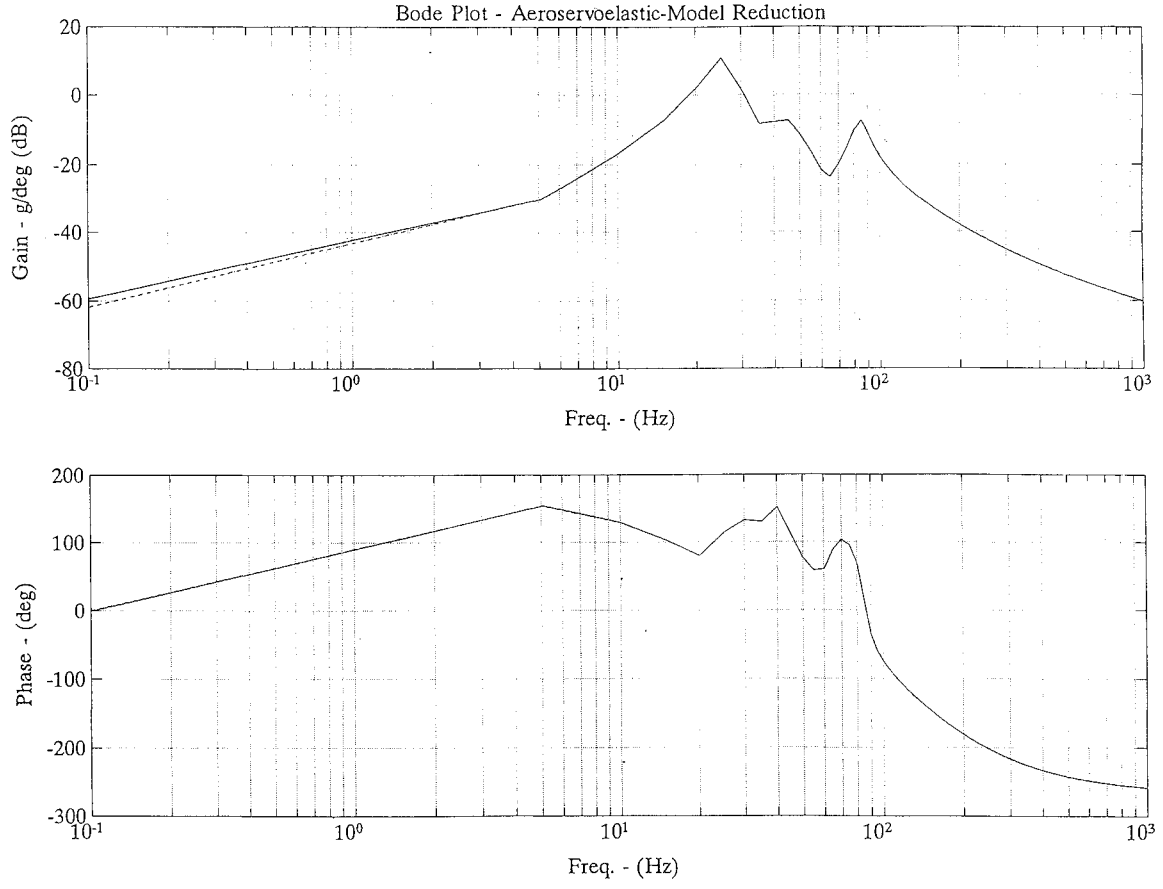

Fig. 3 Aeroservoelastic model reduction: solid line, 16th-order model; dotted line, 11th-order model.

order will be used for controller synthesis purposes, but hereafter, the full-order aeroservoelastic model will be available to evaluate the closed-loop system stability and performance in the simulation tests.

III. Controller Design Methodology

It is well known that the supercritical flutter design point usually gives rise to unstable non-minimum-phase plants with modeling uncertainties in the critical aeroelastic mode frequencies and control effectiveness as well as broad parameter variations with changes in dynamic pressure. Thereby, a very robust control law must be synthesized in order to satisfy these stringent operation conditions.

In recent years it has been shown that an attractive way of representing uncertainties in a plant would be expressed in terms of additive stable perturbations to the factors in the normalized left

Table 1 Full-order controller performances

Case description	k	$\varepsilon_{e,\max}$	$\delta_{\rm rms} \le 1$ deg	$\delta_{\rm rms} \le 90$ deg/s
$W_0 = k$	1.0	0.2511	0.3901	71.750
	2.0	0.3262	0.4420	88.967
	3.0	0.3441	0.4831	114.90
	5.0	0.3409	0.6353	174.79
$W_0(s) = \dfrac{ka}{s+a}$	2.0	0.2927	0.4011	66.256
$W_0(s) = \dfrac{ka}{s+a}\dfrac{s^2+2b_1cs+c^2}{s^2+2b_2cs+c^2}$	2.0	0.2812	0.3946	61.595

coprime factorization of the plant.[10,11] This uncertainty description is rather general as it allows for both zeros and poles crossing into the right-half plane, as would represent uncertainties at the pole locations of lightly damped resonant poles. To introduce performance robustness trade-offs, the design process combines classical open-loop shaping principles with an H_∞ robust stabilization problem in the normalized coprime factors framework. In this paper, a designer selected scalar output weighting function $W_0(s)$ is used for loop-shaping purposes and it is such that the extended plant contains no hidden unstable modes.

Now, a four-block H_∞ robust stabilization problem for the extended plant, $G_e(s) = W_0G(s)$, can be defined as

$$\left\| \begin{bmatrix} K_\Phi S W_0^{-1}(s) & K_\Phi SG(s) \\ S(s) & W_0 SG(s) \end{bmatrix} \right\|_\infty \le \varepsilon_e^{-1} \tag{5}$$

where $S(s) = [I - GK_\Phi(s)]^{-1}$ is the sensitivity function. The suboptimal central controller $K_\Phi(s)$ is characterized by the solution of two generalized algebraic Ricatti equations (GAREs) and a design parameter $\varepsilon_e < \varepsilon_{e,\max}$, as described in Refs. 10 and 11. Additionally, this maximum stability margin, $\varepsilon_{e,\max}$, is given directly as a function of the GARE solutions without the iterative procedure required in classical H_∞ control problems. Thus, the four bounded transfer function in Eq. (5) can be physically interpreted as the maximum output gains for the plant and controller due to input and output disturbances, and $W_0(s)$ becomes a true free design parameter.

Finally, a few comments concerning the robust stability margin ε_e generated with this method are in order. First, it gives a clear indication of the loop-shaping success. Second, it can be interpreted as a measure of robustness because it gives the maximum perturbation size that the extended plant can accommodate on its normalized left coprime factors without becoming unstable. Lastly, it gives bounds on several closed-loop transfer functions of interest during the control law synthesis. It is worth noticing that the final controller is built as $K_e(s) = K_\Phi W_0(s)$.

In this work, a constant weighting was initially considered in order to satisfy the control capacity constraints, and the higher frequency behavior was adjusted by frequency-shaping filters in subsequent steps. The output weighting function $W_0(s)$ was used as a free design parameter in Eq. (5), and a closed-loop trade-off between the control surface activity $K_\Phi S(s)$ and the disturbance attenuation $SG(s)$ was executed.[20] Table 1 shows that as W_0 increases, more control surface activity is permitted, as reflected by the rms values of the control surface deflection and its rate. A value of $W_0 = 2$ was selected, since the upper limit on the control surface rate was violated for higher values.

Note the fact that $G_e(s)$ is not strictly proper for the constant-weighting case, in which case the H_∞ controllers will not be strictly proper. As a consequence, high-frequency noises will be greatly amplified and would overwhelm the actuator unit capacity. Therefore, the weighting function was modified with a first-order filter to weight the control action at frequencies before reaching the actuator bandwidth of 40 Hz. As can be seen from the same table, the control surface activities are reduced by the incorporation of the first-order filter with a break frequency at 35 Hz, and the maximum robust stability margin $\varepsilon_{e,\max}$ is slightly reduced.

Finally, a second-order notch filter was added to heavily weight the control action at 40 Hz to avoid overpower of the actuator unit due to the third elastic mode (first torsional mode) excitations. The control surface activities were predicted to be $\delta = 0.3946$ deg and $\dot{\delta} = 61.595$ deg/s, which are below the specified upper limits of 1 deg and 90 deg/s, respectively. The closed-loop root-locus plot with full-order controller (17th order) is shown in Fig. 4.

The closed-loop flutter dynamic pressure at $M = 0.8$ achieves a value of $qf_{\rm cl} = 34.55$ kPa and the maximum robust stability margin is $\varepsilon_{e,\max} = 0.2812$. The latter represents approximately a 28% of allowable proportional uncertainty in the normalized left coprime factors of the extended plant in the crossover frequency region. It is noted throughout Table 1 that a design parameter ε_e equal to $0.925\varepsilon_{e,\max}$ was used to synthesize the suboptimal controllers. As will be shown in the next section, the selection of the ε value has profound influence on the controller reduction process.

IV. Controller Order Reduction Method

As already stated earlier, the high-order dynamic plants originated from aeroservoelastic formulation transfer the high-order property to the synthesized controller when modern controller design techniques are used. In addition, it is necessary to realize the frequency-shaping filters as part of the controller when loop-shaping principles are applied. In the case of full-order implementation,[21] the required controller attains an order of $n_c = n + 2n_f$, where n is the order of the model and n_f is the order of the frequency-shaping filter. Consequently, given that the order of the resulting controller becomes inevitably large, a two-stage controller reduction process has been considered.[22] In the first stage, the full-order controller will be block diagonalized and residualization techniques will be applied in order to preserve all the important low-frequency modes and replace the less important modes by their static terms, whereas the second stage will be accomplished by the BTA technique as in the aeroservoelastic-model reduction case, which was executed in Sec. II. In the residualization process, the basic idea is to replace the stable high-frequency dynamics portion by their static term (DC gain), generating a feedforward term in the controller output equation as a direct consequence. Then, the 17th-order controller was reduced to a 6th-order controller by residualization. The first two columns in Table 2 show the eigenvalues of the full-order controller and those retained in the controller after the first-stage reduction process. Note that the lowest frequency complex-conjugate pairs are retained in this case.

In the second stage of the order reduction process, the asymptotically stable, residuaized controller $K_{\Phi 1}(s)$ with a minimal realization $(\bar{A}_c, \bar{B}_c, \bar{C}_c, \bar{D}_c)$ is partitioned as

$$\bar{A}_c = \begin{bmatrix} \bar{A}_{c11} & \bar{A}_{c12} \\ \bar{A}_{c21} & \bar{A}_{c22} \end{bmatrix}, \qquad \bar{B}_c = \begin{bmatrix} \bar{B}_{c1} \\ \bar{B}_{c2} \end{bmatrix}, \qquad \bar{C}_c = [\,\bar{C}_{c1} \quad \bar{C}_{c2}\,]$$

where $\bar{A}_{c11} \in R^{k\times k}$, $\bar{B}_{c1} \in R^{k\times m}$, and $\bar{C}_{c1} \in R^{p\times k}$ for $1 \le k \le n_{c1}$. The subsystem $K_{\Phi 2}(s) = (\bar{A}_{c11}, \bar{B}_{c1}, \bar{C}_{c1}, \bar{D}_c)$ is a good approximation of the system $K_{\Phi 1}(s) = (\bar{A}_c, \bar{B}_c, \bar{C}_c, \bar{D}_c)$ if $\sigma_k > \sigma_{k+1}$, where $\sigma_i, i = 1, \ldots, n_{c1}$, are the associated Hankel singular values.[21] Applying the BTA method, two additional states were truncated from the normalized right coprime factors of the residualized controller,

Table 2 Controller reduction process

Full-order controller eigenvalues	First-stage reduction eigenvalues	Second-stage reduction eigenvalues
$-41.78 \pm 53.88i$	$-41.78 \pm 53.88i$	$-41.75 \pm 53.90i$
$-27.69 \pm 222.64i$	$-27.69 \pm 222.64i$	$-27.77 \pm 222.65i$
$-50.26 \pm 246.25i$	$-50.26 \pm 246.25i$	Truncated by BTA
$-31.43 \pm 252.95i$	Residualized	
$-54.29 \pm 304.59i$	Residualized	
$-263.65 \pm 338.00i$	Residualized	
$-29.50 \pm 529.04i$	Residualized	
-219.91	Residualized	
-503.88	Residualized	
-980.79	Residualized	

Table 3 Summary of controller performances

Controller order	$\delta_{rms} \leq 1$ deg	$\delta_{rms} \leq 90$ deg/s	qf_{cl} kPa	Margin increase,[a] %	$\underline{\sigma}_{min}(I + GK_{\Phi})$
17	0.394	61.595	34.55	44.62	0.50 (at 19.3 Hz)
4	0.398	60.424	32.40	35.62	0.46 (at 27.7 Hz)

[a]At $M = 0.8$, $qf_{ol} = 23.89$ kPa.

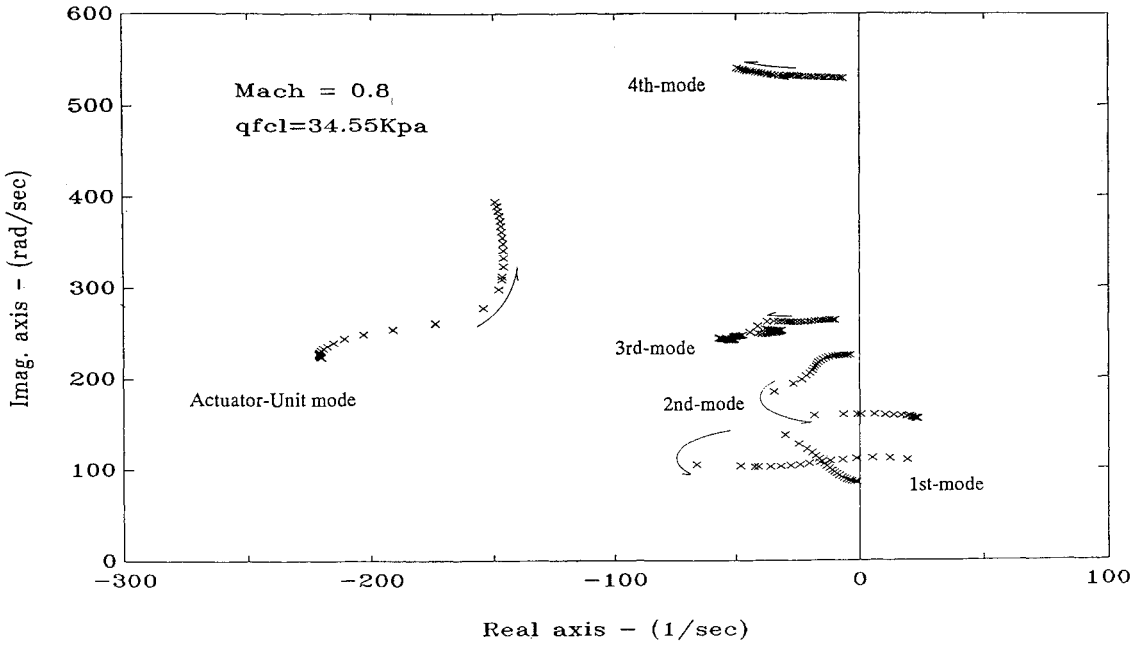

Fig. 4 Closed-loop aeroservoelastic root locus (10 m/s velocity intervals), full-order controller (17th order).

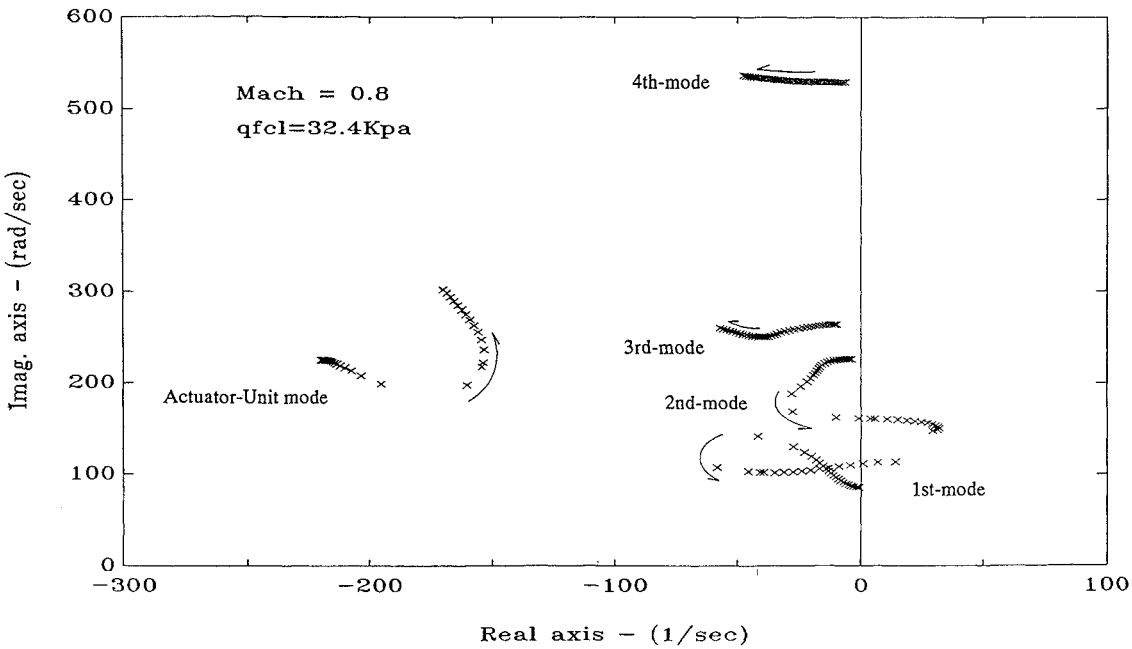

Fig. 5 Closed-loop aeroservoelastic root locus (10 m/s velocity intervals), reduced-order controller (fourth order).

and the resulting reduced-order controller finally achieved four states. The last column of Table 2 shows the resulting eigenvalues of the two-stage reduced-order controller. Their locations in the complex plane are practically unchanged, as can be observed from it. The root locus of the closed-loop aeroservoelastic system is shown in Fig. 5, in which only the elastic modes and actuator unit roots are displayed as a function of velocity.

Table 3 summarizes the closed-loop results achieved with the full-order and the reduced-order controllers, in which δ and $\dot{\delta}$ are evaluated at the supercritical flutter point and qf_{cl} represents the maximum dynamic pressure at which the aeroservoelastic system remains stable. The closed-loop flutter dynamic pressure obtained with the fourth-order controller reached a value of 32.4 kPa, and the control surface activities are well below the specified constraints.

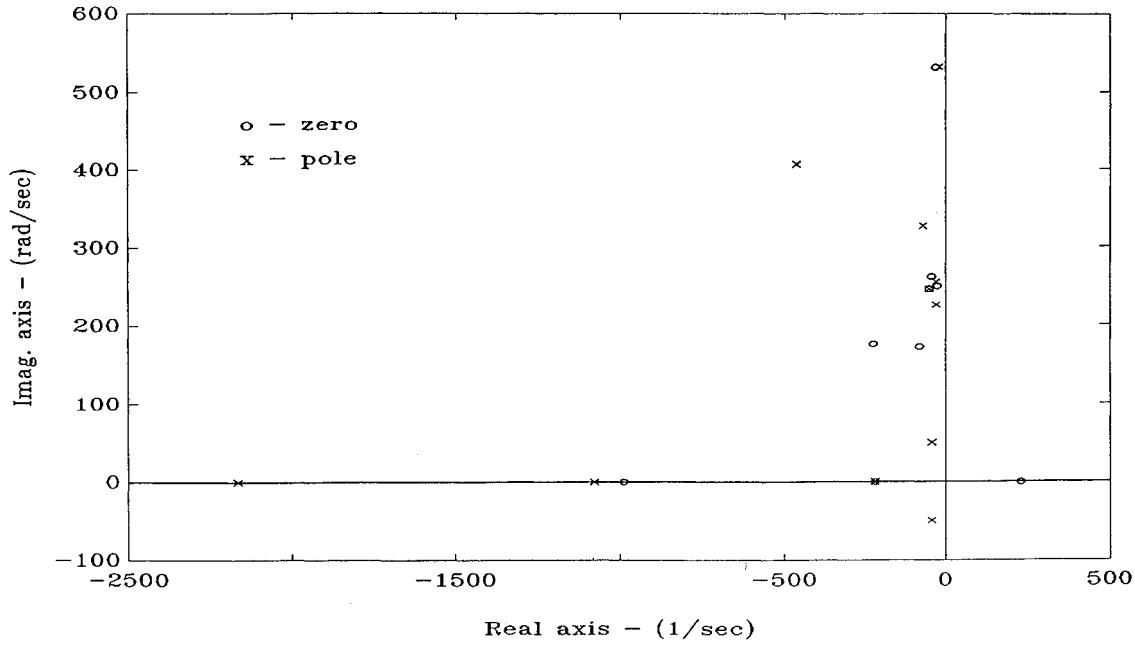

Fig. 6 Full-order H_∞ optimal controller: pole-zero constellation (U = 216 m/s, $\varepsilon = 0.995\varepsilon_{e,\max}$).

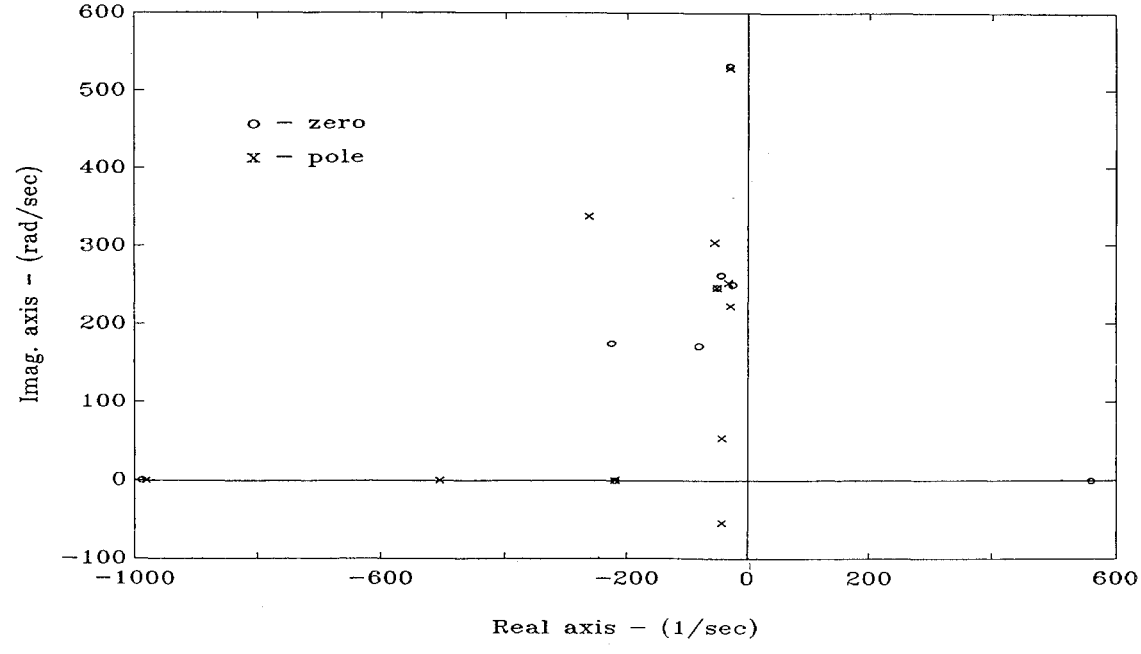

Fig. 7 Full-order H_∞ suboptimal controller: pole-zero constellation (U = 216 m/s, $\varepsilon = 0.925\varepsilon_{e,\max}$).

Also, as a measure of the system stability margin, the minimum singular value of the return difference function $\underline{\sigma}(I + GK_\Phi)$ was computed for both the full-order and reduced 4th-order controllers. Since this is a scalar function (SISO case), it results in the radial distance of the Nyquist locus from the critical −1 point. As can be appreciated, the minimum singular value for the less complex fourth-order control law is slightly deteriorated during the reduction process, and the guaranteed gain or phase margins for the reduced-order control law are determined to be −2.1 dB, +4.2 dB, and ±28 deg, respectively.

Finally, the statement issued in the last paragraph of Sec. III regarding the influence of the design parameter ε_e on the controller reduction process will be addressed. At this end, the design parameter assumes the following values of $\varepsilon_{e,\max}$, e.g., ε_e = 0.925, 0.94, 0.96, 0.98, 0.995 of $\varepsilon_{e,\max}$, and we define hereafter the controller corresponding to $\varepsilon_e = 0.995\varepsilon_{e,\max}$ to be the optimal solution. Figures 6 and 7 display the pole-zero constellations for the optimal and suboptimal controllers synthesized with the design parameter values of ε_e = 0.995, 0.925 of $\varepsilon_{e,\max}$. They clearly show the cancellation of several poles by their neighboring zeros, and the number of pole-zero cancellations are increased as ε_e is reduced (increase the suboptimality). As a direct consequence of this phenomenon, the reduction process is greatly improved without notable degradation of the controller performance during the execution of its duties. Table 4 summarizes the number of pole-zero cancellations that result in the synthesized controllers for each one of the selected ε values. It can be concluded that the total probable number of pole-zero cancellations for $\varepsilon_e = 0.925\varepsilon_{e,\max}$ design case has been completely deleted during the residualization stage.

In addition, when ε_e is reduced, the controller right-half-plane (RHP) zero moves along the real axis, from a position that lies between the origin and the aeroservoelastic model zeros (complex-conjugate pair) to a position behind the model's RHP zeros, as shown in Fig. 8. It is well known that the presence of RHP zeros constrains the bandwidth below which effective disturbance attenuation is possible, that is, for which the sensitivity function can be made small.[23]

Hence, ε_e must also be chosen in order not to impose a new limitation in the range of frequencies over which the use of feedback can be beneficial. For the actual aeroservoelastic control problem, the suboptimal value of $\varepsilon_e = 0.925\varepsilon_{e,\max}$ give rise to a suboptimal H_∞ controller that is easy to reduce and does not limit the achievable performance of the feedback loop, in spite of the inherent restriction dictated by the aeroservoelastic model RHP zeros.

It must be noted that by the two-stage controller reduction process, the controller's real RHP zero was changed to a complex-conjugate pair. The final controller's RHP zeros still remain behind the aeroservoelastic model zeros, and therefore the last statement maintains its validity.

V. Controller Validation

Robust Stability Simulation

The full-order aeroservoelastic model (16th order) was used to evaluate the closed-loop system robust stability at the supercritical flutter condition using the 4th-order suboptimal controller. It is well known that robust stability can be tested by using additive and multiplicative uncertainty descriptions in the frequency domain. Figures 9 and 10 display $1/[\bar{\sigma}(K_{\Phi_2}S)]$ and $1/[\bar{\sigma}(GK_{\Phi_2}S)]$, respectively, that is, the maximum allowable additive and output multiplicative plant perturbations against which the control system would deal. In the former the nominal aeroservoelastic-model gain is shown in dotted lines as well. It is observed that enough additive uncertainty can be permitted at low and high frequencies. Figure 10 indicates that output multiplicative uncertainties near 38% of the aeroservoelastic-model gain may be permitted in the frequency range where the flutter phenomenon is characterized.

Besides the closed-loop frequency-domain indicators, a preliminary parameter sensitivity analysis was carried out by varying the most important parameters associated with the flutter instability in order to evaluate the control law robust characteristics.[24] Accordingly, the predominant natural frequencies that degenerate in the flutter phenomenon were perturbed by ±10% of their nominal value. Table 5 shows these results where ω_1 and ω_2 denotes the first elastic mode (first bending) and second elastic mode (coupled bending and torsional mode) natural frequencies, respectively. As can be noticed from it, the reduced-order controller is ineffective to stabilize the aeroservoelastic model up to the supercritical flutter condition ($1.2qf_{\text{oi}}$) when the second elastic mode natural frequency is decreased. These tests point out that the reduction of this parameter from its nominal value has a strong destabilizing influence over the aeroservoelastic model. As it will be clear during the experimental validation phase, however, the digitalized fourth-order controller can actually stabilize the wing model whose second elastic mode frequency appears to be characterized by a value between the first and second columns of Table 5.

Table 4 Summary of controller pole-zero cancellations

ε_e	0.925	0.940	0.960	0.980	0.995
Number of exact pole-zero cancellations	6	6	4	3	3
Number of nearly exact pole-zero cancellations	2	—	2	2	2
Total probable number of cancellations	8	6	6	5	5

Digital Control Law and Test Set-up

The digital controller has been obtained by applying bilinear transformation to its continuous version, e.g., $z = (1+sT/2)/(1-sT/2)$, where $T = 0.002$ s is the sampling interval. A sketched version of the experimental set-up and flow signals used during the wind-tunnel tests are shown in Fig. 11. As can be seen, the accelerometer signals pass through the antialiasing filter and analog-to-digital (A/D) converter to the digital computer, where the control law is hosted and executed. The appropriate command digital signals from the computer to the active trailing-edge control surface are transformed into continuous ones by the D/A converter device. Strip-chart recorders and a digital spectrum analyzer were used to visualize the sensors and control surface potentiometer signals. Additionally, magnetic-tape recorders were employed for further posttest flutter analysis.

Wind-Tunnel Test Results

At the beginning, open-loop flutter tests were conducted to define the aeroservoelastic wing-model flutter characteristics; e.g., the flutter dynamic pressure and flutter frequency were given as

Table 5 Sensitivity of closed-loop flutter dynamic pressure to parameter perturbations

$\omega_1 \backslash \omega_2$	−10%	Nominal	+10%
−10%	25.74	33.11	42.21
Nominal	25.12	32.40	42.21
+10%	24.50	31.70	42.21

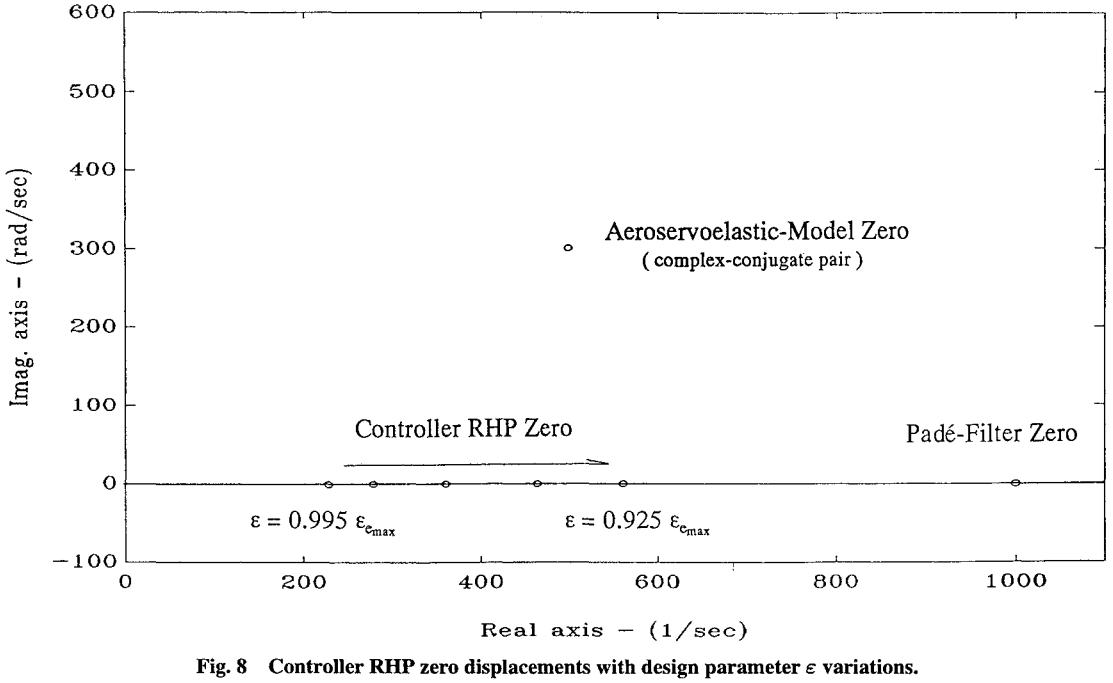

Fig. 8 Controller RHP zero displacements with design parameter ε variations.

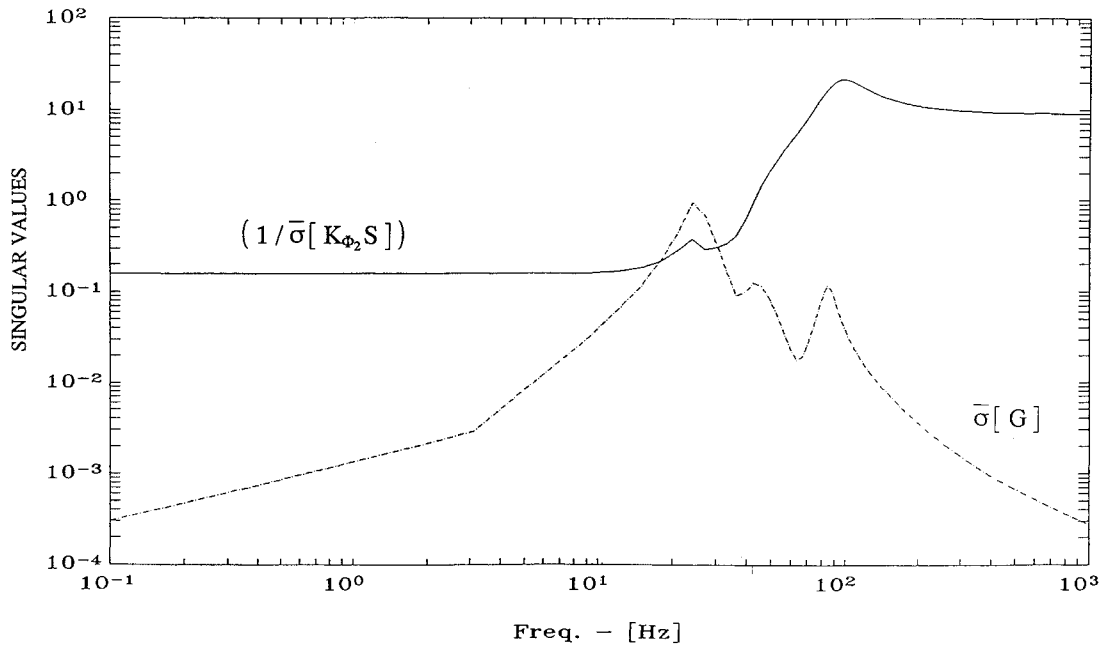

Fig. 9 Allowable additive uncertainty $[1/\bar{\sigma}(K_{\Phi 2}S)]$.

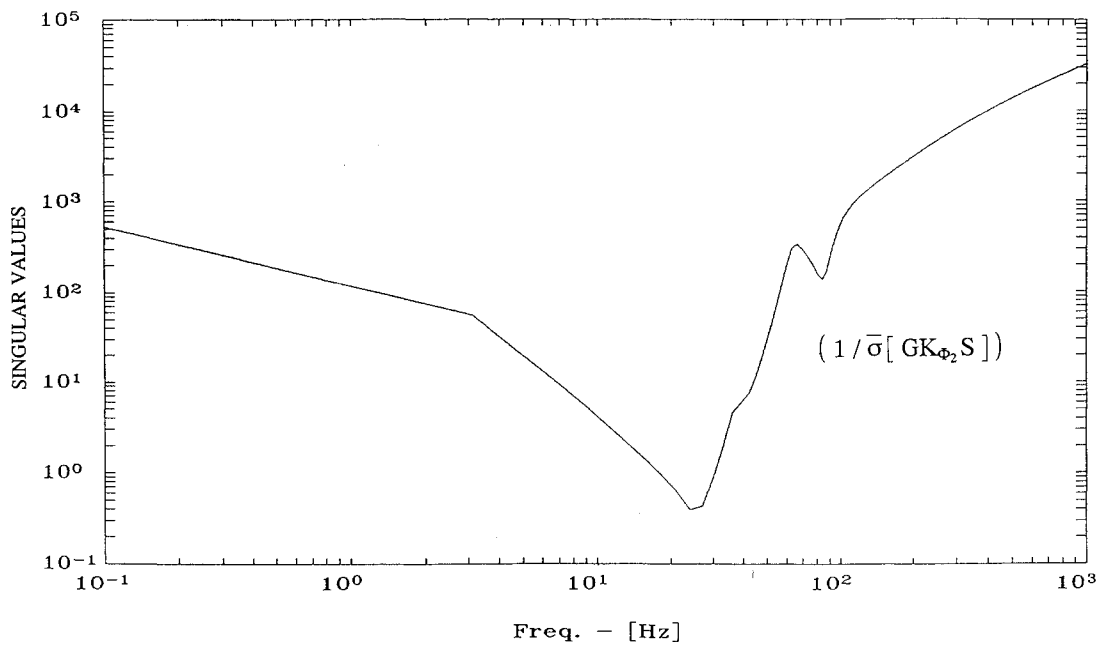

Fig. 10 Allowable output multiplicative uncertainty $[1/\bar{\sigma}(GK_{\Phi 2}S)]$.

a function of Mach number. Subsequently, closed-loop tests were performed to evaluate the synthesized control law effectiveness in actual flutter environments. At Mach 0.8, the open-loop flutter onset was reached at a dynamic pressure of 26.28 kPa and a frequency of 21.6 Hz. These values, when compared with their analytically estimated counterparts, clearly represent off-nominal work conditions for the digitalized control law. These discrepancies would be conferred to the overestimation of the unsteady aerodynamic loads at the transonic dip phenomenon region to the use of a subsonic lifting surface method. Even so, the flutter margin augmentation system successfully extended the actual wing-model open-loop flutter boundary by 11.4%, achieving a dynamic pressure of 29.72 kPa. It is also noted that despite the discrepancies in the predicted values of the fundamental flutter parameters, the control law maintains the closed-loop system stability at the nominal supercritical flutter condition of 28.67 kPa. A more comprehensive description of the flutter tests of the actively controlled aeroservoelastic wing model can be found in Ref. 14.

Figure 12 shows the measured accelerometer output PSD (power spectrum density) due to wind-tunnel turbulence in a subcritical flutter condition (q = 23.37 kPa) for both control-off and control-on situations. In Fig. 12a the first elastic mode frequency is clearly visualized at 19.8 Hz, but the second elastic mode frequency becomes barely visible in a range of frequencies between 22 and 24 Hz. However, when the digital controller was engaged, its interaction with the aeroservoelastic wing model resulted in a decrease down to 15.5 Hz of the first elastic mode frequency and an increase up to 27 Hz of the second elastic mode frequency, without causing modifications in the high-frequency region, as shown in Fig. 12b. Therefore, it is the belief of the authors that the increase of the flutter dynamic pressure is owed to the effective controller action that broadens the range of frequencies of the predominant modes that lead to the flutter phenomenon. It must be noted that the same pattern was appreciated from several measured PSD plots from the strain gauge output, and in addition the same qualitative frequency displacements were verified in posttest analytical simulations.

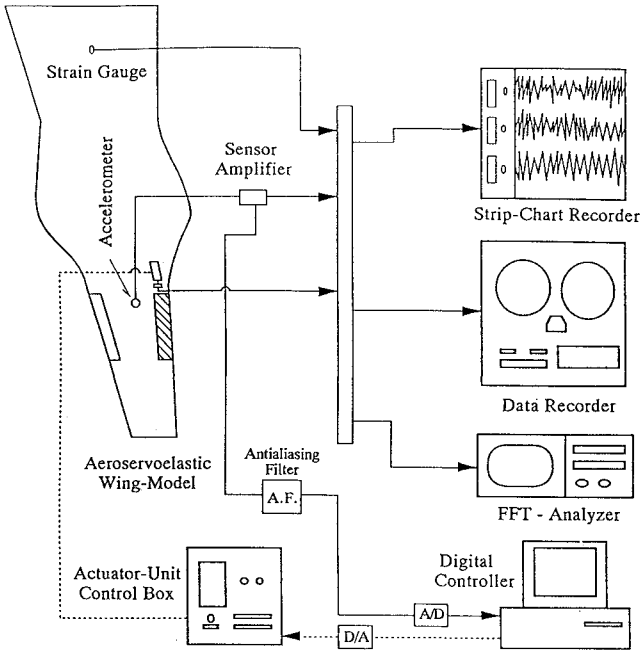

Fig. 11 Test set-up sketch.

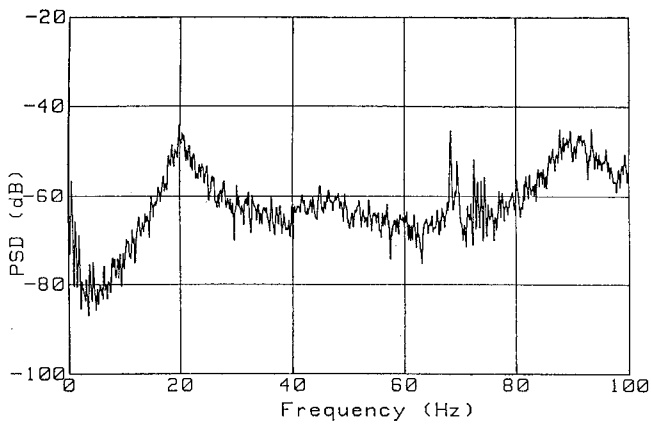

a) Control off

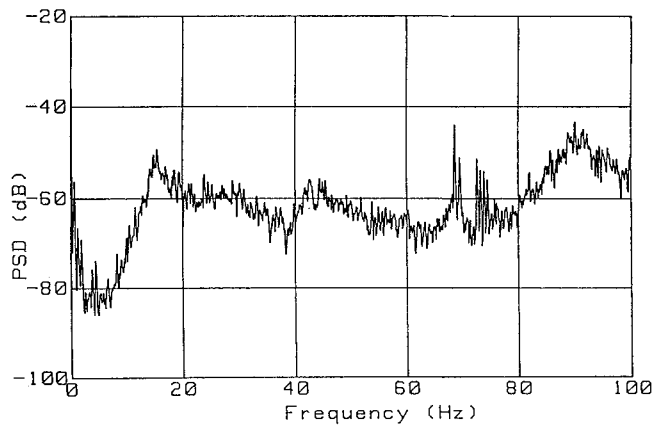

b) Control on

Fig. 12 PSD of accelerometer output at subcritical flutter condition ($M = 0.8$, $q = 23.37$ kPa).

VI. Summary

By solving the robust stabilization problem at the normalized coprime factors framework, the control law for purposes of FMA was synthesized and tested in a transonic wind tunnel. The synthesis methodology proved to be suitable for the design of controllers in the complex aeroservoelastic field.

The main role of the design parameter ε_ϵ on the controller reduction process and on the achievable feedback loop performance was further clarified in this work. Robust stability studies were carried out against additive and output multiplicative plant uncertainties in the frequency domain. Closed-loop parameter sensitivity analyses clearly indicated the destabilizing effect caused by the reduction of the second elastic mode natural frequency from its nominal value. The digital fourth-order controller was successfully tested under stringent off-nominal operating conditions and was shown to stabilize the aeroservoelastic wing model by 11.4% over its actual open-loop flutter boundary. Finally, all discussions in this paper are limited to the SISO system, but the design procedures can deal with a general multiple-input, multiple-output problem as well.

Acknowledgments

The authors express their gratitude to the rest of the members of the Active Control Technology Group at the National Aerospace Laboratory for the invaluable wind-tunnel tests data provided.

References

[1]O'Connell, R. F., and Messina, A. F., "Design, Development and Testing of an Active Flutter Margin Augmentation System for a Commercial Transport Airplane," *Journal of Guidance and Control*, Vol. 3, 1980, pp. 352–360.

[2]Sandford, M. C., Abel, I., and Gray, D. L., "Development and Demonstration of a Flutter-Suppression System Using Active Controls," NASA TR R-450, Dec. 1975.

[3]Schmidt, D. K., and Chen, T. K., "Frequency Domain Synthesis of a Robust Flutter Suppression Control Law," *Journal of Guidance, Control, and Dynamics*, Vol. 9, 1986, pp. 346–351.

[4]Mahesh, J. K., Stone, C. R., Garrard, W. L., and Dunn, H. J., "Control Law Synthesis for Flutter Suppression Using Linear Quadratic Gaussian Theory," *Journal of Guidance and Control*, Vol. 4, 1981, pp. 415–422.

[5]Matsushita, H., Miyazawa, Y., Ueda, T., and Suzuki, S., "Multi-Surface Control Law Synthesis and Wind Tunnel Test Verification of Active Flutter Suppression for a Transport-Type Wing," European Forum on Aeroelasticity and Structural Dynamics (Aachen, Germany), 1989, pp. 1–9 (Paper 89-057).

[6]Matsuzaki, Y., Ueda, T., Miyazawa, Y., and Matsushita, H., "Gust Load Alleviation of a Transport-Type Wing: Test and Analysis," *Journal of Aircraft*, Vol. 26, 1989, pp. 322–327.

[7]Baldelli, D. H., Ohta, H., and Nitta, K., "Gust Load Alleviation of an Aeroelastic Wing Model," *Transactions of the Japan Society for Aeronautical and Space Sciences*, Vol. 36, 1993, pp. 125–142.

[8]Liebst, B. S., and Garrard, W. L., "Design of an Active Flutter Suppression System," *Journal of Guidance, Control, and Dynamics*, Vol. 9, 1986, pp. 64–71.

[9]Perry, B., III, and Miller, G. D., "A Summary of the Active Flexible Wing Program," AIAA Paper 92-2080, April 1992.

[10]Glover, K., and McFarlane, D., "Robust Stabilization of Normalized Coprime Factor Plant Descriptions with H_∞-Bounded Uncertainty," *IEEE Transactions on Automatic Control*, Vol. 34, 1989, pp. 821–830.

[11]McFarlane, D., and Glover, K., "A Loop Shaping Design Procedure Using H_∞ Synthesis," *IEEE Transactions on Automatic and Control*, Vol. 37, 1992, pp. 759–769.

[12]Baldelli, D., Ohta, H., and Matsushita, H., "Robust Stabilization of an Aeroelastic Wing-Model Using the Normalized Coprime Factors Approach," *Proceedings of the 31th Aircraft Symposium*, Japan Society for Aeronautical and Space Sciences, 1993, pp. 74–77.

[13]Doyle, J. C., and Stein, G., "Multivariable Feedback Design: Concepts for a Classical/Modern Synthesis," *IEEE Transactions on Automatic Control*, Vol. 26, 1981, pp. 4–16.

[14]Matsushita, H., Hashidate, M., Saitoh, K., Ando, Y., Suzuki, K., Fujii, K., and Baldelli, D. H., "Transonic Flutter Control of a High Aspect Ratio Wing: Mathematical Modeling, Control Law Design and Wind Tunnel Tests," Paper ICAS-94.5.6.2, Sept. 1994.

[15]Ueda, T., and Dowell, E. H., "A New Solution Method for Lifting Surfaces in Subsonic Flow," *AIAA Journal*, Vol. 20, 1982, pp. 348–355.

[16]Roger, K. L., "Airplane Math Modeling Method for Active Control Design," AGARD-CP-228, 1977, pp. 4.1–11.

[17]Moore, B. C., "Principal Component Analysis in Linear Systems: Controllability, Observability and Model Reduction," *IEEE Transactions on Automatic Control*, Vol. 26, 1981, pp. 17–32.

[18]Mustafa, D., and Glover, K., "Controller Reduction by H_∞ Balanced

Truncation," *IEEE Transactions on Automatic Control*, Vol. 36, 1991, pp. 668–682.

[19]McFarlane, D., Glover, K., and Vidyasagar, M., "Reduced-Order Controller Design Using Coprime Factor Model Reduction," *IEEE Transactions on Automatic Control*, Vol. 35, 1990, pp. 369–373.

[20]Buddie, S. A., Georgiou, T. T., Özgüner, Ü., and Smith, M. C., "Flexible Structure Experiments at JPL and WPAFB: H_∞ Controller Designs," *International Journal of Control*, Vol. 58, No. 1, 1993, pp. 1–19.

[21]McFarlane, D., and Glover, K., "Robust Controller Design Using Normalized Coprime Factor Plant Descriptions," *Lecture Notes in Control and Information Sciences*, Vol. 138, Springer–Verlag, New York, 1989, Chap. 5.

[22]Mukhopadhyay, V., "Flutter Suppresion Digital Control Law Design and Testing for the AFW Wind-Tunnel Model," AIAA Paper 92-2095, April 1992.

[23]Kwakernaak, H., "Robust Control and H_∞ Optimization—Tutorial Paper," *Automatica*, Vol. 29, No. 2, 1993, pp. 255–273.

[24]Waszak, M. R., and Srinathkumar, S., "Flutter Suppresion for the Active Flexible Wing: Control System Design and Experimental Validation," AIAA Paper 92-2097, April 1992.